PROTEINS
STRUCTURE ■ FUNCTION ■ BIOINFORMATICS

Normal-mode-based modeling of allosteric couplings that underlie cyclic conformational transition in F_1 ATPase

Wenjun Zheng*

Department of Physics, University at Buffalo, Buffalo, New York 14260

ABSTRACT

F_1 ATPase, a rotary motor comprised of a central stalk (γ subunit) enclosed by three α and β subunits alternately arranged in a hexamer, features highly cooperative binding and hydrolysis of ATP. Despite steady progress in biophysical, biochemical, and computational studies of this fascinating motor, the structural basis for cooperative ATPase involving its three catalytic sites remains not fully understood. To illuminate this key mechanistic puzzle, we have employed a coarse-grained elastic network model to probe the allosteric couplings underlying the cyclic conformational transition in F_1 ATPase at a residue level of detail. We will elucidate how ATP binding and product (ADP and phosphate) release at two catalytic sites are coupled with the rotation of γ subunit via various domain motions in $\alpha_3\beta_3$ hexamer (including intrasubunit hinge-bending motions in β subunits and intersubunit rigid-body rotations between adjacent α and β subunits). To this end, we have used a normal-mode-based correlation analysis to quantify the allosteric couplings of these domain motions to local motions at catalytic sites and the rotation of γ subunit. We have then identified key amino acid residues involved in the above couplings, some of which have been validated against past studies of mutated and γ-truncated F_1 ATPase. Our finding strongly supports a binding change mechanism where ATP binding to the empty catalytic site triggers a series of intra- and intersubunit domain motions leading to ATP hydrolysis and product release at the other two closed catalytic sites.

Proteins 2009; 76:747–762.

Key words: F_1 ATPase; elastic network model; correlation; allostery; domain motion; normal mode; binding change.

INTRODUCTION

A large variety of multisubunit biomolecular machines share the common architecture of a ring-shaped hexamer with six nucleotide-binding sites located at intersubunit interfaces. These hexameric motors, represented by F_1 ATPase,[1] various hexameric helicases[2,3] and AAA+ proteins,[4] are powered by cooperative binding and hydrolysis of nucleotide to produce diverse mechanical movements involving a central stalk or substrate within the hexamer.

The most studied example of hexameric motors is F_1 ATPase (referred as F_1, hereafter). F_1 is a globular catalytic moiety of F_0F_1-ATP synthase—a giant molecular motor that utilizes the energy of proton motive force across the mitochondrial membrane to synthesize ATP (see a recent review[5]). F_1 forms a hexamer ($\alpha_3\beta_3$) consisting of three β subunits sandwiched between three α subunits,[1] which encloses a central stalk comprised of γδε subunits[6] [see Fig. 1(a)]. Three catalytic sites and three noncatalytic sites are located at the interfaces between adjacent α and β subunits [see Fig. 1(a)]. The former are comprised of highly conserved catalytic residues from β subunit (named cis-residues, including Walker A or P loop motif[8]) and α subunit (named trans-residue, including arginine finger). F_1 hydrolyzes ATP to generate a counterclockwise rotation of γ subunit [as viewed from membrane, see Fig. 1(a)], which was directly visualized by single-molecule microscopy.[9] A clockwise rotation of γ subunit was observed during ATP synthesis in F_0F_1-ATP synthase.[10]

Decades of biochemical studies have firmly established the highly cooperative nucleotide binding and hydrolysis in F_1—both among the three catalytic sites,[11–14] and between the catalytic and noncatalytic sites.[15] To account for the cooperative ATPase in F_1, a "binding change" mechanism[16] has been proposed and widely accepted. It postulates that the γ subunit rotates during ATP hydrolysis to facilitate a cooperative change in the nucleotide-binding affinity of three catalytic sites. However, the mechanistic details of cooperative binding change remain unclear. For example, it has been debated for years whether the cooperativity requires binding of nucleotides at two catalytic sites (bi-site activation[17,18]) or three catalytic sites (tri-site activation[19,20]).

Grant sponsor: University at Buffalo.
*Correspondence to: Wenjun Zheng, Department of Physics, University at Buffalo, 239 Fronczak Hall, Buffalo, NY 14260. E-mail: wjzheng@buffalo.edu.
Received 20 October 2008; Revised 14 January 2009; Accepted 15 January 2009
Published online 2 February 2009 in Wiley InterScience (www.interscience.wiley.com).
DOI: 10.1002/prot.22386

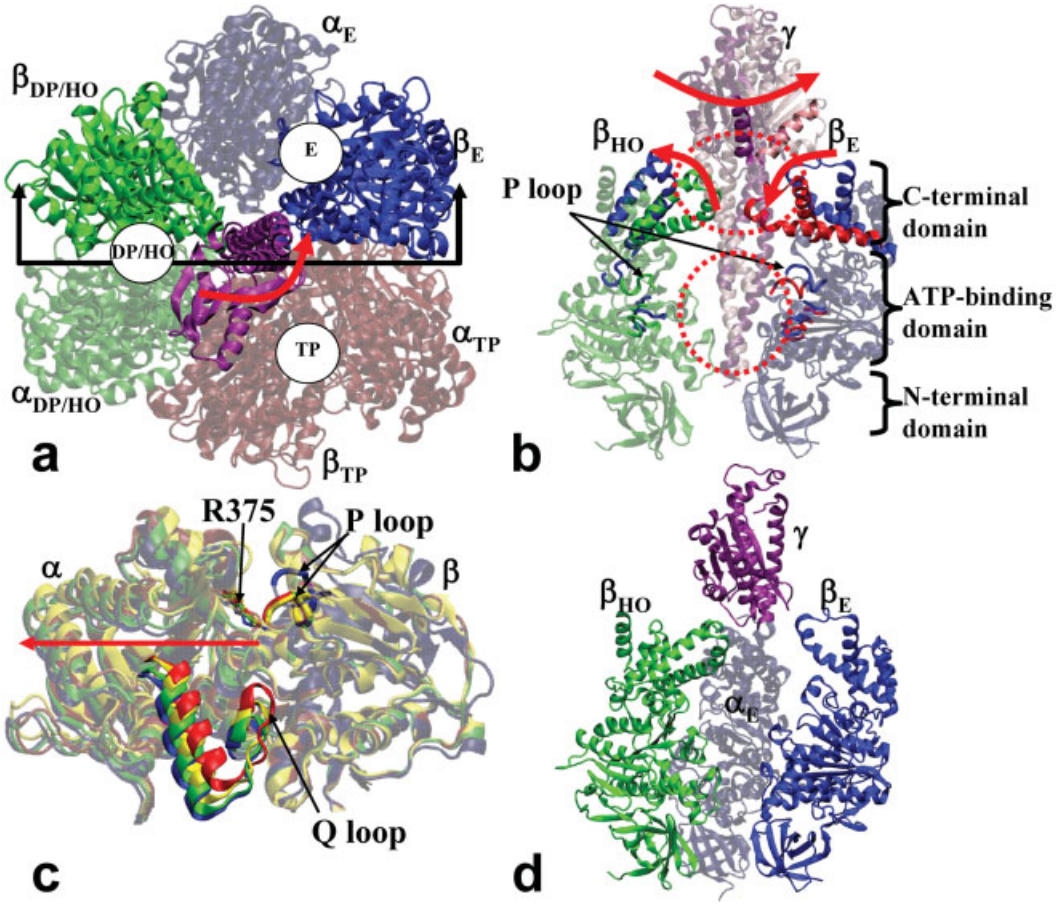

Figure 1

Structural architecture and structure changes of F_1 ATPase. (**a**) Top view of F_1 (viewed from membrane) is shown, including seven subunits ($\alpha_E\beta_E$: blue, $\alpha_{DP/HO}\beta_{DP/HO}$: green, $\alpha_{TP}\beta_{TP}$: red, γ: purple) and three catalytic sites (E, DP/HO, TP). γ, β_E, and $\beta_{DP/HO}$ subunits are shown as opaque cartoons and the remaining subunits as transparent cartoons. The direction of 120° rotation of γ subunit is shown by a red arrow. The side-view direction of panel (b) is shown. (**b**) Side view of observed structural changes in γ, β_E, and β_{HO} subunits of F_1 is shown, including counterclockwise rotation of γ subunit and hinge-bending motions in β_E and β_{HO} subunits (shown by red arrows). Following the same color scheme as panel (a), the beginning (end) conformation of β_E, β_{HO}, and γ subunit is colored blue (red), green (blue), and purple (pink). For clarity, the beginning conformation is shown as transparent cartoons, and only the end conformation of the following structural elements is shown as opaque cartoons—cis-residues of catalytic site (residues 160–165, 187–189, 256–259, and 308–309), the HTH motif of C-terminal domain (residues 365–415), and a helix of γ subunit. The N-terminal domain, ATP-binding domain, and C-terminal domain are labeled. The two sets of contacts between the upper/lower part of γ subunit and the C-terminal/ATP-binding domains of $\alpha_3\beta_3$ hexamer are circled. (**c**) Intersubunit rotations between the ATP-binding domains of $\alpha_E\beta_E$ subunits of 2HLD (blue), $\alpha_{HO}\beta_{HO}$ subunits of 2HLD (green), $\alpha_{TP}\beta_{TP}$ subunits of 2HLD (red), and $\alpha_{DP}\beta_{DP}$ subunits of 1BMF (yellow). The four core helices in β subunits (on the right) are superimposed to show rotations of α subunits (on the left). The following key structural elements are shown as opaque cartoons or bonds—P loop (residues 160–165), Q loop and its adjacent core helix (residues 272–297), and arginine finger (R375). The rest of $\alpha\beta$ subunits are shown as transparent cartoons. The rotational axis is shown by a red arrow. (**d**) Side view of a γ-truncated F_1 structure is shown [same color schemes as panel (b)], where residues 1–25 and 232-end of γ subunit are deleted from 2HLD following Ref. 7.

High resolution structural studies have offered critical support to the binding change mechanism. The landmark crystal structure of bovine F_1[1] (PDB: 1BMF) has captured a snapshot of three structurally distinct catalytic sites. The empty E-site, AMPPNP-bound TP-site and ADP-bound DP-site are located at α_E-β_E, α_{TP}-β_{TP}, and α_{DP}-β_{DP} interface, respectively [see Fig. 1(a)]. E-site and β_E subunit adopt an open conformation. TP-site, DP-site, and associated β subunits (β_{TP} and β_{DP}) are in a closed conformation. Such structural differences explain the heterogeneous nucleotide-binding affinities found by solution measurements,[21,22] which can be attributed to the different interactions between three β subunits and the structurally asymmetric γ subunit.[1] Although the first F_1 structure[1] was later found to be azide-bound and in an ADP-inhibited state,[23] later azide-free F_1 structures have revealed essentially the same asymmetric structural architecture. Meanwhile, structural variations at catalytic

sites were observed in later solved F_1 structures. In an ADP:AlF_4^--inhibited bovine F_1 structure, a "half-closed" catalytic site (named HC-site, and the adjoined α and β subunits are named α_{HC} and β_{HC}, following Ref. 24) bound with ADP and sulfate[25] was found. The HC-site was thought to represent the posthydrolysis, preproduct release step along the catalytic pathway.[25] In another yeast F_1 structure, a "half-open" catalytic site (named HO-site, and the adjoined α and β subunits are named α_{HO} and β_{HO}[24]) bound with AMPPNP was found.[26] The above local structural changes at catalytic sites are accompanied by small rotations of γ subunit,[26] which hints for an allosteric coupling between the opening/closing of a catalytic site and the rotation of γ subunit.

To integrate structural and biochemical data, the three conformations of catalytic sites (E, TP, DP) were assigned to different nucleotide states (with high, medium, and low nucleotide-binding affinity) in various binding change models.[18,27–29] It has been debated whether the high-affinity nucleotide state is assigned to DP-site[1,25,27,28] or TP-site.[18,29,30] The latter scenario has gained supports from recent experiments[31,32] and free energy calculations.[33]

In complement with the static structures of F_1, single-molecule imaging studies have offered valuable information for the F_1 dynamics. The γ subunit undergoes a 120° rotation per ATP hydrolyzed,[34,35] which is resolved into four stages: ATP-waiting dwell, 80° substep following ATP binding, catalytic dwell, and 40° substep linked to release of a hydrolysis product[36,37] (for an alternative pathway with no substeps see Ref. 38). Two catalytic events occur during the catalytic dwell[36]—one is ATP cleavage,[39] the other is assumed to be the release of a hydrolysis product.[36] During the 120° γ rotation, ATP binding and cleavage occur at two different catalytic sites,[37] and a third catalytic event occurs at a third site.[40] Thus, all three catalytic sites participate sequentially to drive the 120° γ rotation.[40] No agreement has been reached on when ADP or phosphate is released during the 120° γ rotation. Whether ADP is released before[41,42] or after[40] the catalytic dwell determines whether the tri-site nucleotide occupancy is transient or kinetically dominant.[43]

Extensive biochemical, structural and dynamic data has provided valuable inputs and constraints for computational modeling of the F_1 dynamics. A variety of computer modeling techniques with different level of structural details have been applied to F_1. Although mechanistic insights were obtained through the kinetic modeling of F_1,[44,45] structure-based molecular simulations are needed to uncover full structural details of F_1 dynamics. All-atom molecule simulations were utilized in free energy calculations of nucleotide binding,[33,46] QM/MM calculations of catalysis,[47,48] and molecular dynamics (MD) simulations of structural changes in F_1.[49–52] The past MD simulations were focused on how the forced rotation of γ subunit in the direction of ATP synthesis induces conformational changes in the $\alpha_3\beta_3$ hexamer. The conformational dynamics of F_1 during ATP hydrolysis has been less studied (see Refs. 23 and 52), because of the difficulty of simulating the structural effects of ATP binding. In addition, the MD simulations of F_1 have been limited to nanoseconds timescale, whereas the ATPase cycle of F_1 spans at least milliseconds. To overcome the barrier of high computing cost for "long-time" MD simulations, coarse-grained modeling has been pursued using simplified energy functions and structural representations (for example, all atoms in an amino acid residue are represented by its C_α atom).[54] For instance, Go models[55] have been widely used in protein folding simulations (see a review[56]) and more recently in simulating conformational transitions in F_1.[53] Another prime example of coarse-grained models is the elastic network model (ENM) which represents a protein structure as a network of C_α atoms locally connected by springs. In an ENM, the all-atom force fields are replaced by simple harmonic potentials with a uniform force constant.[57–59] Early studies have shown that the large-scale collective motions predicted by the normal mode analysis (NMA) of ENM are insensitive to the dramatic simplification in ENM.[60–62] The low-frequency modes calculated from ENM were found to compare well with many large-scale domain motions observed crystallographically.[62,63] Numerous studies have established the ENM as an efficient means to tease out the functionally relevant conformational dynamics from biomolecular structures with virtually no limit in timescale or system size (see reviews[64–66]). Indeed, ENM has been applied to large biomolecular complexes such as ribosome,[67,68] chaperonin GroEL,[69,70] viral capsids,[71,72] and most recently F_1.[24]

This study is in part motivated by two recent studies of F_1 dynamics during hydrolysis using coarse-grained modeling, which have reached contradicting conclusions. In one study,[53] Koga and Takada used a switching Go model to simulate conformational transitions in F_1. They concluded that ATP binding and ADP release are tightly coupled in a single kinetic process during the 80° substep, and phosphate release from DP-site accompanies the 40° substep. Their results support an always bi-site model (nucleotide occupancy is always two).[53] In another study,[24] Pu and Karplus used a PNM-based targeted dynamics simulation to explore how the γ subunit responds to induced structural changes in the $\alpha_3\beta_3$ hexamer following a two-stage transition. They concluded that ATP binding triggers an 80° rotation of γ subunit in the first stage, whereas product release accompanies a 40° rotation of γ subunit in the second stage. Their results agree with a tri-site model (nucleotide occupancy alternates between two and three).[43]

Besides using different simulation techniques, the two studies[24,53] made different assumptions for structural intermediates during the 120° γ rotation. Koga and Takada

built hybrid intermediate structures from the 1994 bovine F_1 structure[1] and the 2001 bovine F_1 structure,[25] whereas Pu and Karplus assumed that the 2001 structure[25] represents the catalytic-dwell state[36,37] and a yeast F_1 structure[26] captures the ATP-waiting state.[36,37] Clearly, their modeling results critically depend on the quality of the presumed structural intermediates. It remains uncertain how well the existing crystallographic structures capture the intermediate states of F_1 in solution (it was argued that some crystallographic forms of F_1 may not be present in solution[73]). Therefore, it is desirable to model the sequence of structural events during the 120° γ rotation without assuming any structural intermediate other than the beginning and end state (ATP-waiting state).

To re-evaluate the conflicting results from the above studies,[24,53] we will perform a normal-mode-based modeling of allosteric couplings in F_1 using a C_α-only ENM (see Methods section). We will analyze allosteric couplings near the beginning and end state of the conformational transition accompanying the 120° γ rotation (both states are represented by the *same* yeast F_1 structure,[26] which contains 3121 amino acid residues or C_α atoms in chains A-G). We will analyze how ATP binding and product release at two catalytic sites are coupled to the rotation of γ subunit via various domain motions (including intrasubunit hinge-bending motions in β subunits and intersubunit rigid-body rotations between adjacent α and β subunits). To this end, we will employ an ENM-based correlation analysis[74] to quantify the correlation between specific motions of two structural components of a protein, which is calculated as a weighted sum of ENM modes (see Methods section). Based on this calculation, we can evaluate the significance of coupled structural changes observed from structural comparisons, and predict whether they occur at the early or late stage of a conformational transition (see Methods section). Additionally, we will identify key residues involved in the allosteric couplings in F_1, some of which will be validated against past studies of mutated and γ-truncated F_1.

METHODS

Elastic network model

In an ENM, a protein structure is represented as a network of C_α atoms of amino acid residues. A harmonic potential with a uniform force constant k accounts for elastic interactions between C_α atoms within a cutoff distance R_c (its default value is 10 Å, and we also examine R_c = 9 Å−12 Å to ensure the robustness of our results). To accurately model the rotational dynamics of γ subunit in F_1, we postulate that the elastic interactions between $\alpha_3\beta_3$ and γ subunit only exist between two residues in atomic contact (with minimal distance between heavy atoms <4 Å). The elastic interactions within $\alpha_3\beta_3$ or γ subunit exist between two residues whose C_α–C_α distance is $<R_c$.

The potential energy of ENM is

$$E = \frac{1}{2}\sum_{d_{ij}^0 < R_c} k\left(d_{ij} - d_{ij}^0\right)^2, \quad (1)$$

where d_{ij} is the distance between the C_α atom i and j, and d_{ij}^0 is the corresponding distance in the crystal structure. We then expand the above potential energy to second order:

$$E \approx \frac{1}{2}\delta X^T H_0 \delta X, \quad (2)$$

where $\delta X = X - X_0$, X is a $3N$-dimensional vector representing the Cartesian coordinates of the N C_α atoms, X_0 is the corresponding vector in the crystal structure, $H_0 = \nabla^2 E|_{X=X_0}$ is the Hessian matrix.

An NMA of the Hessian matrix yields $3N$-6 nonzero normal modes (excluding six zero modes corresponding to three rotations and three translations), which are numbered from 1 to $3N$-6 in order of ascending eigenvalue. To validate ENM, a normal mode m is compared with the observed structural changes between two crystal structures (represented by a $3N$-dimensional vector ΔR) by calculating an overlap $I_m = \frac{\Delta R^T V_m}{|\Delta R|\cdot|V_m|}$, where V_m is the eigenvector of mode m, $|\Delta R|$ and $|V_m|$ represent the amplitudes of ΔR and V_m. In addition, a cumulative overlap $C_M = \sqrt{\sum_{m=1}^{M} I_m^2}$ is calculated to assess how well the lowest M modes describe ΔR. C_M^2 gives the percentage of the observed structural changes (ΔR) captured by the lowest M modes.

Correlation analysis of coupled motions involving two structural components

We have recently developed a correlation analysis to quantify the coupling between the specific motions of two structural components (S1 and S2) of a protein complex.[74] The correlation between the two given movements of S1 and S2 (represented by two $3N$-dimensional displacement vectors X_1 and X_2, which are normalized to unit amplitude) is calculated by summing up contributions from individual modes:

$$C_{12} = \sum_{m \le M} \frac{X_1^T V_m \cdot V_m^T X_2}{\lambda_m}, \quad (3)$$

where M is the cutoff mode ($M = 3N$-6 by default), V_m and λ_m are the eigenvector and the eigenvalue of mode m. A positive (or negative) C_{12} means that the two movements are correlated (or anti-correlated). A major advantage of the correlation analysis is that it captures the net effects of low-frequency structural fluctuations without requiring the dominance of a few modes.

The two movements of S1 and S2 (represented by two $3N$-dimention vectors X_1 and X_2) are obtained by super-

imposing two protein conformations along the C_α atoms of S1 and S2 at the beginning state and the end state of a conformational transition. In general, the correlation (Eq. 3) is computed using the ENM modes solved at both the beginning state and the end state: at the beginning (end) state, X_1 and X_2 are obtained by a structural superposition using the beginning (end) conformation as a reference structure. The order of atomic coordinates in X_1 and X_2 follows that of the eigenvectors of ENM modes. The nonzero elements of X_1 and X_2 differ depending on whether the beginning or the end conformation is used as a reference structure. In case of F_1, both the beginning state and the end state correspond to the same yeast F_1 structure,[26] so the ENM modes are only calculated once for this structure. A strongly positive C_{12} at the beginning state (or end state) suggests that the two motions involving S1 and S2 are coupled at the early (or late) stage of the transition. On the contrary, a weakly positive or negative C_{12} at the beginning state (or end state) implies that either or both movements do not occur at the early (or late) stage of the transition. Therefore, the correlation analysis can qualitatively predict coupled motions involved in the early or late stage of a conformational transition.

Perturbation analysis to identify key residues involved in coupled motions

To identify the key residues involved in a given coupling, we introduce a residue-position-specific perturbation δk to the force constant of springs connecting a given residue position n to its neighbors.[75] This perturbation results in the following change to the Hessian matrix:

$$\delta H_n = \delta k \sum_{d_{ni}^0 < R_c} H_{ni}, \qquad (4)$$

where $H_{ni} = \nabla^2[(d_{ni} - d_{ni}^0)^2/2]|_{X-X_0}$ is contributed by the interaction between residue n and i.

Then the first-order perturbation theory predicts that the resulting change in the correlation C_{12} (at cutoff mode $M = 3N$-6) is

$$\delta C_{12}(n) = -\delta k \sum_{d_{ni}^0 < R_c} X_1^T H^{-1} H_{ni} H^{-1} X_2, \qquad (5)$$

where $H^{-1} = \sum_{m=1\ldots3N-6} \frac{V_m V_m^T}{\lambda_m}$.

$$|\delta C_{12}(n)| \le \delta k \cdot S_n,$$

where $S_n = \sum_{d_{ni}^0 < R_c} |X_1^T H^{-1} H_{ni} H^{-1} X_2|$. Therefore, the importance of a residue position n to the correlation C_{12} is assessed by the S_n score. We will sort all residue positions of F_1 in order of decreasing S_n and keep the top 100 residues as key residues involved in C_{12}. Mutational perturbations to these residue positions are expected to compromise the allosteric coupling described by C_{12}.

To complement the above first-order perturbation analysis which only applies to small perturbations, we will also analyze the effects of large perturbations. To assess whether the contacts between two structural elements (for example, the γ subunit and the C-terminal domain of β_{TP} subunit in F_1) are important to a given correlation, the elastic interactions between them are turned off and the correlation (Eq. 3) is recomputed using the normal modes of the "perturbed" ENM. The involvement of the chosen contacts in the given correlation is evaluated by how much the correlation is reduced by the perturbation. We will use this analysis to determine what contacts between the γ subunit and the $\alpha_3\beta_3$ hexamer are critically involved in the allosteric couplings in F_1.

RESULTS AND DISCUSSION

Low-frequency modes collectively capture the cyclic conformational change in F_1

As clearly revealed by the first bovine F_1 structure,[1] the cooperative binding change[16] involves a cyclic structural change in three catalytic sites (E → TP → DP → E) and adjoined $\alpha\beta$ subunits accompanied by a 120° counterclockwise rotation of γ subunit [see Fig. 1(a)]. The cyclic structural change can be deduced by superimposing the bovine F_1 structure onto itself such that the six subunits[1] (α_E, β_E, α_{TP}, β_{TP}, α_{DP}, and β_{DP}) are aligned in a cyclic manner ($\alpha_E\beta_E\alpha_{TP}\beta_{TP}\alpha_{DP}\beta_{DP}$ → $\alpha_{TP}\beta_{TP}\alpha_{DP}\beta_{DP}\alpha_E\beta_E$). This prevailing structural picture remains unchanged after more F_1 structures were solved with minor structural variations compared with the 1994 F_1 structure[1] (except two F_1 structures[76,77]).

To model the cyclic structural change of F_1, we will follow Ref. 24 and use a yeast F_1 structure[26] (PDB: 2HLD) instead of the 1994 structure[1] (PDB: 1BMF) for the following reasons: first, 1BMF is in an ADP-inhibited state,[23] and it may have captured the catalytic-dwell state between the 80° and 40° substeps[80] rather than the ATP-waiting state at the beginning of the cyclic structural transition; second, more residues of γ subunit are resolved in 2HLD than in 1BMF, which allows a better description of interactions between γ subunit and $\alpha_3\beta_3$ hexamer. With 2HLD replacing 1BMF, the DP-site is replaced by HO-site, and the cyclic structural change is represented as $\alpha_E\beta_E\alpha_{TP}\beta_{TP}\alpha_{HO}\beta_{HO}$ → $\alpha_{TP}\beta_{TP}\alpha_{HO}\beta_{HO}\alpha_E\beta_E$ [see Fig. 1(a)].

An ADP:AlF_4^--inhibited bovine F_1 structure[25] (PDB: 1H8E) was proposed to have captured the catalytic-dwell state between the 80° and 40° substeps.[24] In this structure, all three catalytic sites (HC, DP, and TP) are nucleotide-bound.[25] The half-closed HC-site is thought to represent a posthydrolysis state[25] which is transformed to E-site upon product release.[24] Thus, the cyclic structural transition is divided into two stages[24]: first, from 2HLD to 1H8E ($\alpha_E\beta_E\alpha_{TP}\beta_{TP}\alpha_{HO}\beta_{HO}$ → $\alpha_{TP}\beta_{TP}\alpha_{DP}\beta_{DP}\alpha_{HC}\beta_{HC}$);

second, from 1H8E to 2HLD ($\alpha_{TP}\beta_{TP}\alpha_{DP}\beta_{DP}\alpha_{HC}\beta_{HC} \rightarrow \alpha_{TP}\beta_{TP}\alpha_{HO}\beta_{HO}\alpha_{E}\beta_{E}$). Unlike Ref. 24, we will not use 1H8E for most of our modeling on allosteric couplings (see "Correlation analysis of allosterically coupled motions in F_1" section), except when we evaluate the proposals that 1H8E captures a structural intermediate during ATP binding or product release (see "Couplings between hinge-bending motions and γ subunit rotation" subsection).

The cyclic structural change involves the following intra- and intersubunit domain motions:

a. Two intrasubunit hinge-bending movements between the C-terminal domains (residues 358–475) and the ATP-binding domains (residues 83–357) of β_E and β_{HO} subunits by ~30° [see Fig. 1(b)]: one is from an open to a closed conformation ($\beta_E \rightarrow \beta_{TP}$), and the other is from a closed to an open conformation ($\beta_{HO} \rightarrow \beta_E$). There is no significant structural change between β_{TP} and β_{HO} subunits. Thus the hinge-bending motions are coupled to nucleotide (ATP or ADP) binding or release in F_1.[79] These hinge-bending motions are thought to be mechanically coupled to the rotation of γ subunit like a camshaft.[44,80] A smaller rotation (~16°) was found between the C-terminal domain of β_{HC} subunit[25] and that of β_E subunit, which suggests that the β_{HC} conformation is intermediate between β_{HO} and β_E conformations.
b. Two intersubunit rigid-body rotations between the ATP-binding domains of adjacent α and β subunits by ~8° (α_E-$\beta_E \rightarrow \alpha_{TP}$-$\beta_{TP}$, α_{TP}-$\beta_{TP} \rightarrow \alpha_{HO}$-$\beta_{HO}$) [see Fig. 1(c)]. There is no significant rotation between the α_E-β_E and α_{HO}-β_{HO} subunit pairs. Therefore, the observed intersubunit rotations are likely in response to the presence or absence of γ-phosphate at the catalytic site between the adjoined α and β subunits.

The above four domain motions are accompanied by the following local motions at three catalytic sites [E-site at α_E-β_E interface, HO-site at α_{HO}-β_{HO} interface, and TP-site at α_{TP}-β_{TP} interface, see Fig. 1(a)]:

a. E → TP: It involves a closing motion between P loop (residues 160–165) and the remaining cis-residues (residues 187–189, 256–259, and 308–309) in β_E subunit, which may result from ATP binding at E-site [see Fig. 1(b)]. It may be coupled to the closing hinge-bending motion in β_E subunit ($\beta_E \rightarrow \beta_{TP}$) as suggested by a dynamical domain analysis[81] (this coupling will be assessed in "Couplings between hinge-bending motions and catalytic sites" subsection).
b. HO → E: It involves an opening motion between P loop and the remaining cis-residues in β_{HO} subunit, which may result in product (ADP or phosphate) release [see Fig. 1(b)]. This local motion was thought to be coupled to the opening hinge-bending motion in β_{HO} subunit ($\beta_{HO} \rightarrow \beta_E$)[81] (this coupling will be assessed in "Couplings between hinge-bending motions and catalytic sites" subsection).
c. TP → HO: It involves a small shift between the cis-residues (including P loop) in β_{TP} subunit and the arginine finger (R375) in α_{TP} subunit [see Fig. 1(c)]. The arginine finger is believed to play a critical role in transition-state stabilization[82,83] and communication between catalytic sites.[84,85] This local intersubunit motion was thought to be coupled to the α_{TP}-$\beta_{TP} \rightarrow \alpha_{HO}$-$\beta_{HO}$ rotation[79] (this coupling will be assessed in "Couplings between intersubunit rotations and catalytic sites" subsection).

To validate the use of ENM-based modeling in F_1, we will verify that the cyclic structural change is captured collectively by the low-frequency ENM modes. Indeed, 56% of the cyclic conformational change is captured by the lowest 100 modes, i.e. ~1% of the total 9363 modes [see Fig. 2(a)], although it is not dominated by a single mode. The most significant mode is #4, which only accounts for ~10% of the cyclic structural change. A similar result was obtained in an earlier NMA of F_1 using an all-atom force field.[86] The finding that multiple modes are needed to capture the cyclic structural change in F_1 prevents us from deducing functional motions by analyzing one dominant mode. To overcome this difficulty, we will analyze dynamic quantities like correlations (see Methods section) instead of selected modes by properly treating contributions from all ENM modes (see "Correlation analysis of allosterically coupled motions in F_1" section).

To assess the proposal that the ADP:AlF_4^--inhibited bovine F_1 structure[25] (PDB: 1H8E) captures an intermediate structure during the cyclic structural transition,[24] we have compared the conformational change from 2HLD to 1H8E with the ENM modes solved for 2HLD. A higher percentage (71%) of the above conformational change is captured by the lowest 100 modes [see Fig. 2(b)]. Therefore, a transition from 2HLD to 1H8E is favored by the low-frequency modes more than the cyclic structural change [see Fig. 2(a)], which supports the above proposal.[24]

Correlation analysis of allosterically coupled motions in F_1

The key question we will address is: how are the nucleotide-dependent local motions at catalytic sites coupled to the rotation of γ subunit to attain cooperative binding change?[16] Structural comparisons suggest that various domain motions may be involved in the above couplings, including the hinge-bending motions in β subunits [$\beta_E \rightarrow \beta_{TP}$ and $\beta_{HO} \rightarrow \beta_E$, see Fig. 1(b)] and the rigid-body rotations between adjacent α and β subunits [α_E-$\beta_E \rightarrow \alpha_{TP}$-$\beta_{TP}$ and α_{TP}-$\beta_{TP} \rightarrow \alpha_{HO}$-$\beta_{HO}$, see Fig. 1(c)]. We will quantitatively evaluate the relevance of these domain motions to the allosteric couplings between catalytic sites

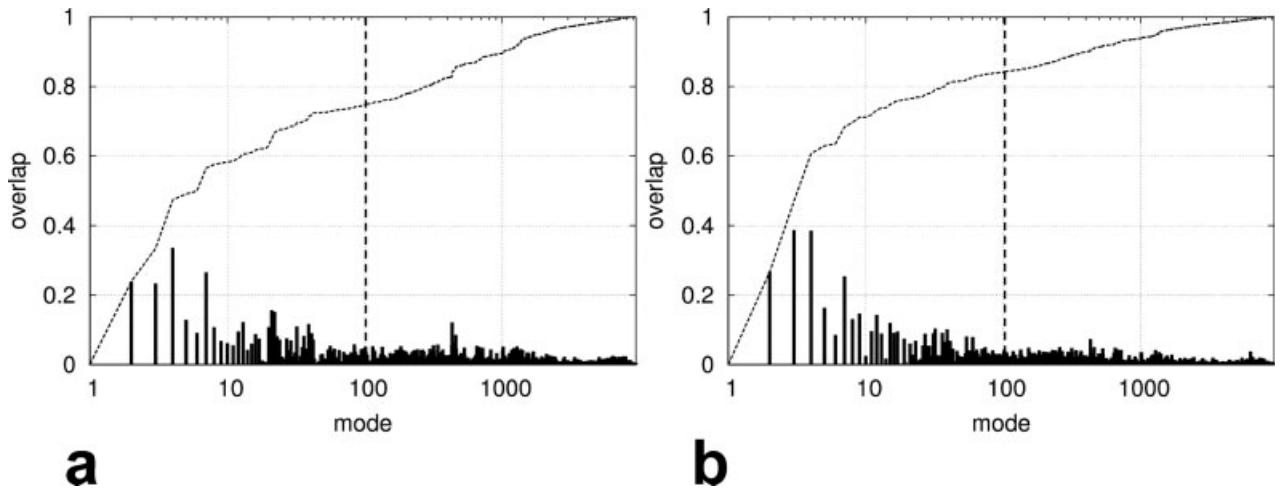

Figure 2

Comparison between ENM modes and the following structural changes in F_1: (**a**) cyclic structural change ($\alpha_E\beta_E\alpha_{TP}\beta_{TP}\alpha_{HO}\beta_{HO} \rightarrow \alpha_{TP}\beta_{TP}\alpha_{HO}\beta_{HO}\alpha_E\beta_E$ of 2HLD); (**b**) transition to an intermediate structure[25] ($\alpha_E\beta_E\alpha_{TP}\beta_{TP}\alpha_{HO}\beta_{HO}$ of 2HLD $\rightarrow \alpha_{TP}\beta_{TP}\alpha_{DP}\beta_{DP}\alpha_{HC}\beta_{HC}$ of 1H8E). The dashed curve shows the cumulative overlap as a function of cutoff mode (see Methods section) and the impulses show the overlap for each mode (see Methods section). The mode number is shown in logarithmic scale to clearly show the positions and overlaps of low-frequency modes.

and γ subunit. To this end, we will employ an ENM-based correlation analysis[74] (see Methods section) to quantify the couplings between the local motions at catalytic sites and the above domain motions (see "Couplings between hinge-bending motions and catalytic sites" and "Couplings between intersubunit rotations and catalytic sites" subsections), together with the couplings between the rotation of γ subunit and those domain motions (see "Couplings between hinge-bending motions and γ subunit rotation" and "Couplings between intersubunit rotations and γ subunit rotation" subsections).

Couplings between hinge-bending motions and catalytic sites

The catalytic site of F_1 is located at the hinge region[81] between the C-terminal domain and the ATP-binding domain of a β subunit [see Fig. 1(b)]. Therefore, the local motion at a catalytic site can be coupled to the hinge-bending motion in the adjoined β subunit.[44,80]

To assess the couplings between hinge-bending motions and catalytic sites near both the beginning and the end conformation of the cyclic structural transition of F_1, we have calculated four correlations ($C^{\beta}_{E\rightarrow TP}$, $C^{\beta}_{TP\rightarrow E}$, $C^{\beta}_{HO\rightarrow E}$ and $C^{\beta}_{E\rightarrow HO}$) between four hinge-bending motions in β subunits ($\beta_E \rightarrow \beta_{TP}$, $\beta_{TP} \rightarrow \beta_E$, $\beta_{HO} \rightarrow \beta_E$, and $\beta_E \rightarrow \beta_{HO}$) and four local motions at catalytic sites (E → TP, TP → E, HO → E, and E → HO). Among them, $C^{\beta}_{E\rightarrow TP}$ and $C^{\beta}_{HO\rightarrow E}$ ($C^{\beta}_{TP\rightarrow E}$ and $C^{\beta}_{E\rightarrow HO}$) pertain to the early (late) stage of the transition. We have found positive correlations in all four cases with different strength (see rows 2–5 of Table I). A much stronger $C^{\beta}_{E\rightarrow TP}$ than $C^{\beta}_{TP\rightarrow E}$ indicates that the two closing motions of E-site and β_E subunit are only coupled at the early stage of the cyclic structural transition when β_E subunit is near β_E conformation of the yeast F_1 structure.[26] On the contrary, a much stronger $C^{\beta}_{E\rightarrow HO}$ than $C^{\beta}_{HO\rightarrow E}$ suggests that the two opening motions of HO-site and β_{HO} subunit are only coupled at the late stage of the cyclic structural transition when β_{HO} subunit is near β_E conformation. These results support the order of E-site closing followed by HO-site opening, which agrees with the proposal that ATP binding drives the energy-requiring opening of β_{HO} subunit and enables product release from HO-site.[33]

Couplings between intersubunit rotations and catalytic sites

At a catalytic site in F_1, the local intersubunit motions between the cis-residues and the arginine finger [see Fig.

Table I
Correlations Between Domain Motions Within $\alpha_3\beta_3$ and Catalytic Sites in F_1

Correlation	Movement of S1	Movement of S2	Dominant modes
$C^{\beta}_{E\rightarrow TP} \approx 1.1$	$\beta_E \rightarrow \beta_{TP}$	E → TP	#4
$C^{\beta}_{TP\rightarrow E} \approx 0.076$	$\beta_{TP} \rightarrow \beta_E$	TP → E	None
$C^{\beta}_{HO\rightarrow E} \approx 0.10$	$\beta_{HO} \rightarrow \beta_E$	HO → E	None
$C^{\beta}_{E\rightarrow HO} \approx 1.2$	$\beta_E \rightarrow \beta_{HO}$	E → HO	#4
$C^{\alpha\beta}_{E\rightarrow TP} \approx 0.046$	$\alpha_E-\beta_E \rightarrow \alpha_{TP}-\beta_{TP}$	E → TP	#4
$C^{\alpha\beta}_{TP\rightarrow E} \approx -0.033$	$\alpha_{TP}-\beta_{TP} \rightarrow \alpha_E-\beta_E$	TP → E	None
$C^{\alpha\beta}_{TP\rightarrow HO} \approx 0.0075$	$\alpha_{TP}-\beta_{TP} \rightarrow \alpha_{HO}-\beta_{HO}$	TP → HO	None
$C^{\alpha\beta}_{HO\rightarrow TP} \approx 0.021$	$\alpha_{HO}-\beta_{HO} \rightarrow \alpha_{TP}-\beta_{TP}$	HO → TP	None

Table II
Correlations Between Domain Motions Within $\alpha_3\beta_3$ and γ Subunit Rotation in F_1

Correlation	Movement of S1	Movement of S2	Dominant modes
$C^{\gamma\text{-}\beta}_{E\to TP} \approx 0.076$	$\beta_E \to \beta_{TP}$	counterclockwise γ rotation	#4-#7
$C^{\gamma\text{-}\beta}_{TP\to E} \approx 0.19$	$\beta_{TP} \to \beta_E$	clockwise γ rotation	None
$C^{\gamma\text{-}\beta}_{HO\to E} \approx 1.1$	$\beta_{HO} \to \beta_E$	counterclockwise γ rotation	#5
$C^{\gamma\text{-}\beta}_{E\to HO} \approx -0.12$	$\beta_E \to \beta_{HO}$	clockwise γ rotation	#4-#7
$C^{\gamma\text{-}\alpha\beta}_{E\to TP} \approx 0.46$	$\alpha_E-\beta_E \to \alpha_{TP}-\beta_{TP}$	counterclockwise γ rotation	#4
$C^{\gamma\text{-}\alpha\beta}_{TP\to E} \approx 0.11$	$\alpha_{TP}-\beta_{TP} \to \alpha_E-\beta_E$	clockwise γ rotation	#5
$C^{\gamma\text{-}\alpha\beta}_{TP\to HO} \approx -0.0027$	$\alpha_{TP}-\beta_{TP} \to \alpha_{HO}-\beta_{HO}$	counterclockwise γ rotation	#5
$C^{\gamma\text{-}\alpha\beta}_{HO\to TP} \approx 0.35$	$\alpha_{HO}-\beta_{HO} \to \alpha_{TP}-\beta_{TP}$	clockwise γ rotation	#4, #5

1(c)] allow the arginine finger to coordinate the γ-phosphate of ATP and facilitate ATP hydrolysis.[1] These local motions may be coupled to the intersubunit rigid-body rotations observed during the cyclic structural change [see Fig. 1(c)].

To separate intersubunit rigid-body rotations from intrasubunit hinge-bending motions, we superimpose the "rigid cores" of two ATP-binding domains from $\alpha_E\beta_E$, $\alpha_{HO}\beta_{HO}$, or $\alpha_{TP}\beta_{TP}$ subunit pairs. The rigid core consists of four helices (residues 211–225, 241–262, 272–287, and 299–309 of an α subunit; or residues 190–204, 225–246, 258–270, and 284–294 of a β subunit). The structures of rigid cores are essentially unchanged between different α or β subunits, so the conformational change deduced by superimposing the rigid cores from adjacent α and β subunits captures the rigid-body rotation between them.

To probe the couplings between intersubunit rotations and catalytic sites near both the beginning and the end conformation of the cyclic structural transition of F_1, we have calculated four correlations ($C^{\alpha\beta}_{E\to TP}$, $C^{\alpha\beta}_{TP\to E}$, $C^{\alpha\beta}_{TP\to HO}$, and $C^{\alpha\beta}_{HO\to TP}$) between four intersubunit rotations (α_E-$\beta_E \to \alpha_{TP}$-β_{TP}, α_{TP}-$\beta_{TP} \to \alpha_E$-β_E, α_{TP}-$\beta_{TP} \to \alpha_{HO}$-$\beta_{HO}$, and α_{HO}-$\beta_{HO} \to \alpha_{TP}$-$\beta_{TP}$) and four local motions at catalytic sites (E → TP, TP → E, TP → HO, and HO → TP) (see rows 6–9 of Table I). Among them, $C^{\alpha\beta}_{E\to TP}$ and $C^{\alpha\beta}_{TP\to HO}$ ($C^{\alpha\beta}_{TP\to E}$ and $C^{\alpha\beta}_{HO\to TP}$) pertain to the early (late) stage of the transition. The finding of positive $C^{\alpha\beta}_{E\to TP}$ and negative $C^{\alpha\beta}_{TP\to E}$ suggests that the two motions (α_E-$\beta_E \to \alpha_{TP}$-β_{TP} and E → TP) are likely to be coupled only at the early stage of the cyclic structural transition when $\alpha_E\beta_E$ subunits are near $\alpha_E\beta_E$ conformation of the yeast F_1 structure.[26] On the contrary, a weaker $C^{\alpha\beta}_{TP\to HO}$ than $C^{\alpha\beta}_{HO\to TP}$ indicates that the two motions (α_{TP}-$\beta_{TP} \to \alpha_{HO}$-$\beta_{HO}$ and TP → HO) are more likely to be coupled at the late stage than the early stage of the cyclic structural transition. The above results support the order of E-site closing (E → TP, associated with ATP binding) followed by TP-site opening (TP → HO, associated with ATP hydrolysis). This order agrees with the single-molecule finding that ATP hydrolysis occurs during the catalytic dwell following the 80° substep induced by ATP binding.[36,39]

Couplings between hinge-bending motions and γ subunit rotation

Signaling between two catalytic sites of F_1 can be transmitted through the intervening α subunit [such as α_E subunit between E-site and HO-site, see Fig. 1(a)] or the rotating γ subunit. Although there is experimental evidence for both signaling schemes,[87,88] we will focus on the latter one. This is because the latter scheme involves collective domain motions (rotation of γ subunit and various domain motions in $\alpha_3\beta_3$ hexamer, see "Low-frequency modes collectively capture the cyclic conformational change in F_1" section) captured by the low-frequency modes, whereas the former scheme may involve local structural changes at α-β interfaces which are generally not well captured by the low-frequency modes.

Following the finding of allosteric couplings between catalytic sites and hinge-bending motions in β subunits (see "Couplings between hinge-bending motions and catalytic sites" subsection), we will assess how the hinge-bending motions are subsequently coupled to the rotation of γ subunit near both the beginning and the end conformation of the cyclic structural transition of F_1. Such couplings have been proposed to be critical to cooperative catalysis and torque generation in F_1,[42,80] but the underlying structural mechanism remains elusive. We have computed four correlations ($C^{\gamma\text{-}\beta}_{E\to TP}$, $C^{\gamma\text{-}\beta}_{TP\to E}$, $C^{\gamma\text{-}\beta}_{HO\to E}$, and $C^{\gamma\text{-}\beta}_{E\to HO}$) between four hinge-bending motions ($\beta_E \to \beta_{TP}$, $\beta_{TP} \to \beta_E$, $\beta_{HO} \to \beta_E$, and $\beta_E \to \beta_{HO}$) and the counterclockwise or clockwise rotation of γ subunit (relative to the N-terminal domains of $\alpha_3\beta_3$ hexamer). Among them, $C^{\gamma\text{-}\beta}_{E\to TP}$ and $C^{\gamma\text{-}\beta}_{HO\to E}$ ($C^{\gamma\text{-}\beta}_{TP\to E}$ and $C^{\gamma\text{-}\beta}_{E\to HO}$) pertain to the early (late) stage of the transition. The results are summarized as follows (see rows 2–5 of Table II):

a. The finding of weak correlations for both $C^{\gamma\text{-}\beta}_{E\to TP}$ and $C^{\gamma\text{-}\beta}_{TP\to E}$ suggests that β_E closing and counterclockwise γ rotation are unlikely to be coupled near the beginning or the end state of the cyclic structural transition. A weak $C^{\gamma\text{-}\beta}_{E\to TP}$ results from cancellation between positively contributing modes (modes #4, #7) and negatively contributing modes (modes #5, #6). Therefore,

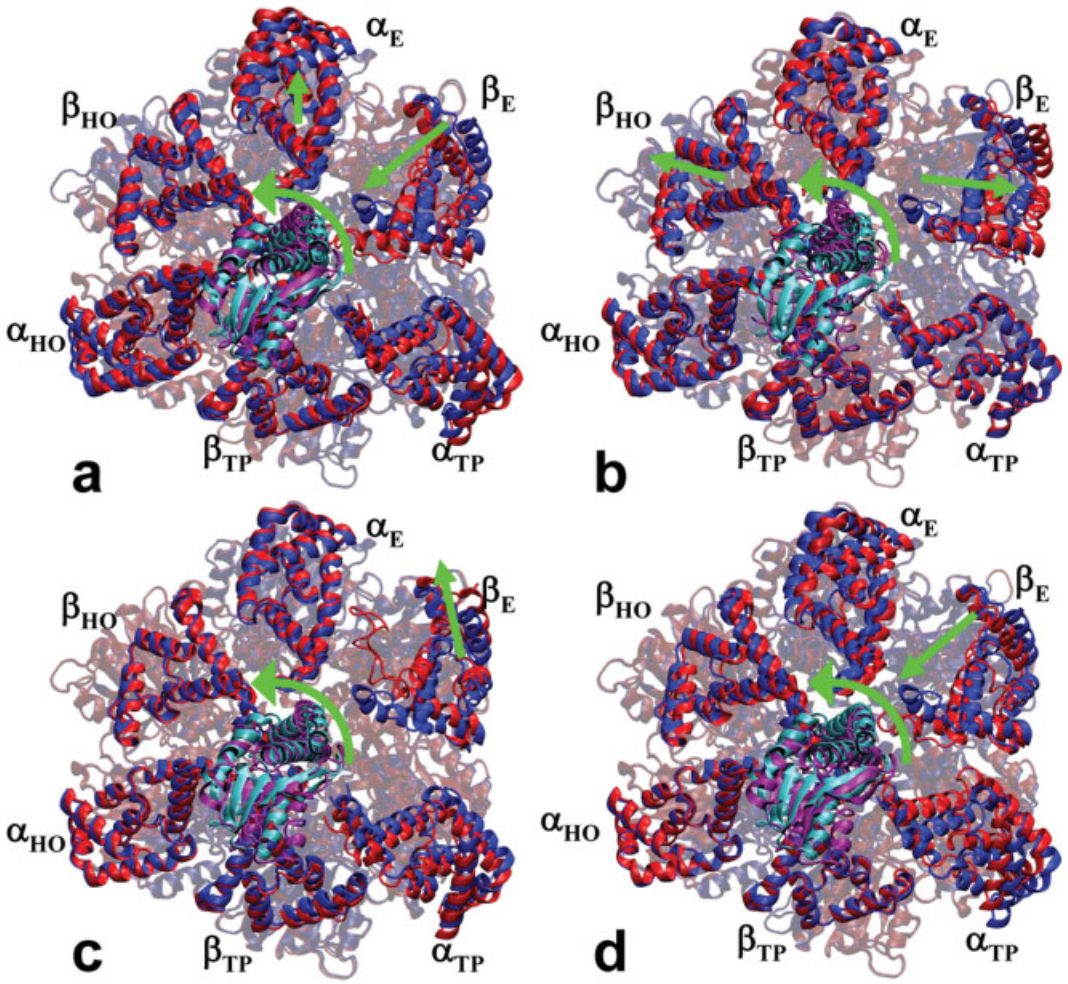

Figure 3

Domain motions described by the following ENM modes: (**a**) #4, (**b**) #5, (**c**) #6, and (**d**) #7. The F_1 crystal structure (PDB: 2HLD) and the deformed F_1 structure (following a displacement in the direction of a given ENM mode) are shown. The former (latter) structure is colored blue (red) in $\alpha_3\beta_3$ hexamer, cyan (purple) in γ subunit. The movements of C-terminal domains of $\alpha_3\beta_3$ hexamer and γ subunit (shown as opaque cartoons) are marked by green arrows. The rest of F_1 is shown as transparent cartoons.

the closing hinge-bending motion in β_E subunit can be coupled to both counterclockwise (via modes #4, #7) and clockwise (via modes #5, #6) γ rotation. The lack of directional bias is necessary for F_1 to function as both an ATPase and an ATP synthase—the former requires a counterclockwise γ rotation accompanied by ATP binding that closes β_E subunit, whereas the latter requires a clockwise γ rotation accompanied by ADP or phosphate binding that closes β_E subunit.

b. The finding of strongly positive $C^{\gamma\text{-}\beta}_{HO\to E}$ and negative $C^{\gamma\text{-}\beta}_{E\to HO}$ indicates that the opening hinge-bending motion in β_{HO} subunit is coupled to the counterclockwise γ rotation only at the early stage of the cyclic structural transition. Such coupling allows the latter to drive the energy-requiring opening of β_{HO} subunit.[50] However, since $\beta_{HO} \rightarrow \beta_E$ is only weakly coupled to the opening of HO-site (see "Couplings between hinge-bending motions and catalytic sites" subsection), product release at HO-site can only occur at the late stage of the cyclic structural transition.

To view the collective motions underlying the above couplings, we have further analyzed the domain motions described by modes #4, #5, #6, and #7 [see Fig. (3a–d)]. Modes #4 and #7 describe an inward (or outward) motion of the C-terminal domain of β_E subunit, accompanied by counterclockwise (or clockwise) γ rotation [see Fig. 3(a,d)]. These collective motions clearly couple $\beta_E \rightarrow \beta_{TP}$ with counterclockwise γ rotation. Mode #5 describes outward (or inward) motions of the C-terminal domains of both β_E and β_{HO} subunits, accompanied by counterclockwise (or clockwise) γ rotation [see Fig. 3(b)]. These motions explain the coupling between $\beta_{HO} \rightarrow \beta_E$ and counterclockwise γ rotation [see Fig. 3(c)].

Mode #6 describes an outward (or inward) motion of the C-terminal domain of β_E subunit in a direction roughly perpendicular to the β_E motion in mode #5, accompanied by counterclockwise (or clockwise) γ rotation [see Fig. 3(c)]. Together with mode #5, it couples the closing of β_E subunit with clockwise γ rotation.

The allosteric couplings between $\alpha_3\beta_3$ hexamer and γ subunit can be transmitted via two sets of intersubunit interactions [see circled regions in Fig. 1(b)]: first, between the C-terminal domains of $\alpha_3\beta_3$ hexamer and the upper part of γ subunit; second, between the ATP-binding domains of $\alpha_3\beta_3$ hexamer and the lower part of γ subunit. To assess the importance of these interactions to the strong coupling between $\beta_{HO} \rightarrow \beta_E$ and counterclockwise γ rotation ($C^{\gamma\text{-}\beta}_{HO\rightarrow E}$), we have performed the correlation analysis on a "perturbed" ENM (see Methods section) as follows:

a. After turning off the first set of interactions, $C^{\gamma\text{-}\beta}_{HO\rightarrow E}$ decreases sharply from 1.1 to -0.14, which indicates their importance to $C^{\gamma\text{-}\beta}_{HO\rightarrow E}$. To identify which α or β subunit is involved in this correlation, we then turn off the interactions between γ subunit and the C-terminal domain of a selected α or β subunit. It is found that the largest decrease in $C^{\gamma\text{-}\beta}_{HO\rightarrow E}$ (from 1.1 to -0.21) occurs when the γ-β_{TP} interactions are turned off. The γ-β_{TP} interactions involve residues *L83*, C84, *G85*, S86, Q117, *R120*, *N239*, *A240*, *N243*, *A244*, *M247* of γ subunit and *D386*, *A389*, *I390*, *L391*, *D394*, *E395*, *E398* of β_{TP} subunit (underlined residues are highly conserved with conservation score ≥ 8[89]). Interestingly, $C^{\gamma\text{-}\beta}_{HO\rightarrow E}$ increases from 1.1 to 1.7 after the γ-β_{HO} interactions are turned off. Therefore, the γ-β_{HO} interactions "lock" β_{HO} subunit in a closed conformation and must be broken to allow γ rotation to drive the opening of β_{HO} subunit.
b. After turning off the second set of interactions, $C^{\gamma\text{-}\beta}_{HO\rightarrow E}$ is nearly unchanged, which suggests that these interactions are not essential to $C^{\gamma\text{-}\beta}_{HO\rightarrow E}$.

The above finding of key γ-$\alpha_3\beta_3$ interactions involving the upper rather than lower part of γ subunit agrees with a recent study of a γ-truncated F_1 with intact rotational characteristics.[7] We have recalculated $C^{\gamma\text{-}\beta}_{HO\rightarrow E}$ using the ENM modes solved for the γ-truncated F_1 structure [see Fig. 1(d)]. Compared with the γ-intact F_1 structure, the correlation is reduced from 1.1 to 0.56 but still persists in the γ-truncated F_1 structure.

To refine the perturbation analysis with a residue level of detail, we have introduced a residue-position-specific perturbation in the elastic interactions and have calculated the resulting change in the correlation (see Methods section). The residues with the largest change are identified as key residues involved in the correlation. In agreement with the above results, many of the key residues involved in $C^{\gamma\text{-}\beta}_{HO\rightarrow E}$ are clustered at the interfaces between the C-terminal domains of $\alpha_3\beta_3$ hexamer and γ subunit [see Fig. 4(a,b)]. Some are distributed at α_{HO}-β_{HO} and α_E-β_{HO} interfaces [see Fig. 4(a,b)]. Some (including residues 172–175 in β_{HO} subunit) are located in the hinge region of β_{HO} subunit, which was found to be functionally important by past mutational studies.[90–93] For example, the defect of an *E. coli* mutant βS174F (low torque and low ATPase) was suppressed by a second site mutation βI166A (corresponding to the key residue I174 of yeast F_1) in the same subunit.[92] Another key residue D315 was verified by the finding that an *E. coli* mutant βD301V (corresponding to D315 of yeast F_1) was defective in ATPase and a βD301E mutation changed the rate-limiting step of the ATPase reaction.[94] Further mutational studies will test the prediction that these key residues couple γ rotation with product release.

Next, we will apply the correlation analysis to an ADP:AlF_4^--inhibited bovine F_1 structure[25] (PDB: 1H8E) and evaluate the proposals that the half-closed β_{HC} conformation represents a structural intermediate during ATP binding ($\beta_E \rightarrow \beta_{HC} \rightarrow \beta_{TP}$) or product release ($\beta_{HO} \rightarrow \beta_{HC} \rightarrow \beta_E$).[25,31,32] We have calculated two correlations ($C^{\gamma\text{-}\beta}_{HC\rightarrow E}$ and $C^{\gamma\text{-}\beta}_{HC\rightarrow TP}$) between two domain motions ($\beta_{HC} \rightarrow \beta_E$ and $\beta_{HC} \rightarrow \beta_{TP}$) and counterclockwise γ rotation using the ENM modes solved for 1H8E.

a. A positive correlation $C^{\gamma\text{-}\beta}_{HC\rightarrow E} = 0.57$ suggests that counterclockwise γ rotation is coupled to the opening of β_{HC} subunit to enable product release from HC-site.[25] This result agrees with the observation of a 40° counterclockwise γ rotation accompanying product release.[36]
b. A negative correlation $C^{\gamma\text{-}\beta}_{HC\rightarrow TP} = -4.3$ suggests that clockwise instead of counterclockwise γ rotation is coupled to the closing of β_{HC} subunit induced by ATP binding to HC-site. This result contradicts the observation of an 80° counterclockwise γ rotation induced by ATP binding.[36]

The above findings support β_{HC} conformation as a structural intermediate involved in product release[25] but not ATP binding. An unknown partially-closed β conformation different from β_{HC} may be involved to facilitate counterclockwise γ rotation driven by ATP binding.

Couplings between intersubunit rotations and γ subunit rotation

Following the finding of allosteric couplings between catalytic sites and intersubunit rotations (see "Couplings between inter-subunit rotations and catalytic sites" subsection), we will assess how the intersubunit rotations are subsequently coupled to the rotation of γ subunit near both the beginning and the end conformation of the cyclic structural transition of F_1. These intersubunit rigid-body rotations (~8°) are smaller than the intrasubunit hinge-bending motions (~30°), and their functional roles were less explored than the latter in previous studies.

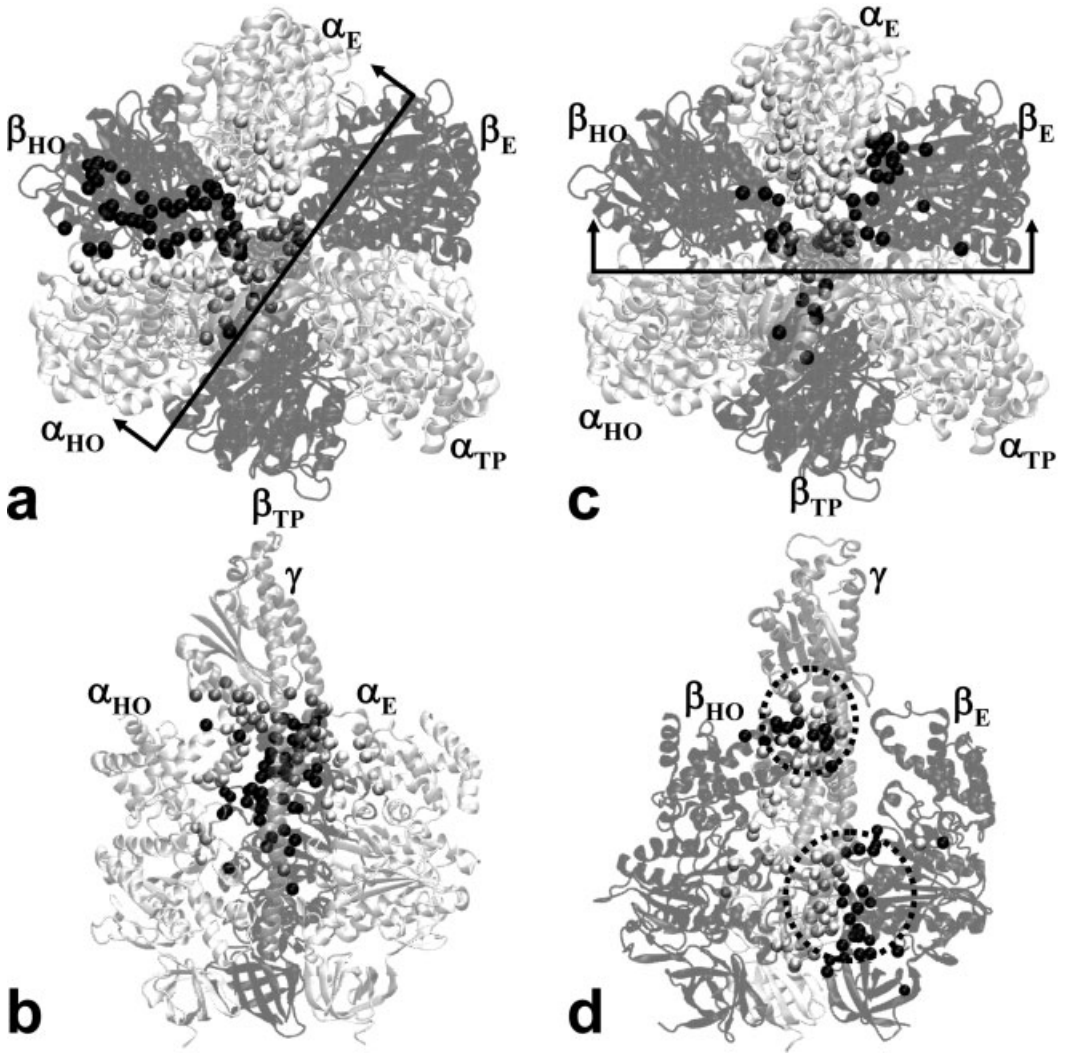

Figure 4

Key residues involved in the following two correlations in F_1: (1) between the hinge-bending motion $\beta_{HO} \rightarrow \beta_E$ and counterclockwise γ rotation (**a**, **b**); (2) between the intersubunit rotation α_E-$\beta_E \rightarrow \alpha_{TP}$-$\beta_{TP}$ and counterclockwise γ rotation (**c**, **d**). Panels (a) and (c) show the top view of all subunits; panel (b) shows the side view of α_{HO}, β_{HO}, α_E, and γ subunits; panel (d) shows the side view of β_{HO}, α_E, β_E, and γ subunits. α, β, and γ subunits are colored white, black, and silver, respectively. The top 100 key residues are shown as spheres and listed in Table III.

We have computed four correlations ($C^{\gamma\text{-}\alpha\beta}_{E\rightarrow TP}$, $C^{\gamma\text{-}\alpha\beta}_{TP\rightarrow E}$, $C^{\gamma\text{-}\alpha\beta}_{TP\rightarrow HO}$, and $C^{\gamma\text{-}\alpha\beta}_{HO\rightarrow TP}$) between four intersubunit rotations (α_E-$\beta_E \rightarrow \alpha_{TP}$-$\beta_{TP}$, α_{TP}-$\beta_{TP} \rightarrow \alpha_E$-$\beta_E$, α_{TP}-$\beta_{TP} \rightarrow \alpha_{HO}$-$\beta_{HO}$, and α_{HO}-$\beta_{HO} \rightarrow \alpha_{TP}$-$\beta_{TP}$) and the counterclockwise or clockwise rotation of γ subunit. Among them, $C^{\gamma\text{-}\alpha\beta}_{E\rightarrow TP}$ and $C^{\gamma\text{-}\alpha\beta}_{TP\rightarrow HO}$ ($C^{\gamma\text{-}\alpha\beta}_{TP\rightarrow E}$ and $C^{\gamma\text{-}\alpha\beta}_{HO\rightarrow TP}$) pertain to the early (late) stage of the transition. The results are summarized as follows (see rows 6–9 of Table II):

a. The finding of a much stronger $C^{\gamma\text{-}\alpha\beta}_{E\rightarrow TP}$ than $C^{\gamma\text{-}\alpha\beta}_{TP\rightarrow E}$ suggests that the α_E-$\beta_E \rightarrow \alpha_{TP}$-$\beta_{TP}$ rotation and counterclockwise γ rotation are coupled only at the early stage of the cyclic structural transition when $\alpha_E\beta_E$ subunits are near $\alpha_E\beta_E$ conformation of the yeast F_1 structure.[26]

b. The finding of a strongly positive $C^{\gamma\text{-}\alpha\beta}_{HO\rightarrow TP}$ and a weakly negative $C^{\gamma\text{-}\alpha\beta}_{TP\rightarrow HO}$ suggests that the α_{TP}-$\beta_{TP} \rightarrow \alpha_{HO}$-$\beta_{HO}$ rotation and counterclockwise γ rotation are coupled only at the late stage of the cyclic structural transition when $\alpha_{TP}\beta_{TP}$ subunits are near $\alpha_{HO}\beta_{HO}$ conformation.

Following "Couplings between hinge-bending motions and γ subunit rotation" subsection, we have assessed the importance of interactions between $\alpha_3\beta_3$ hexamer and γ subunit [see Fig. 1(b)] to the strong coupling between α_E-$\beta_E \rightarrow \alpha_{TP}$-$\beta_{TP}$ and counterclockwise γ rotation ($C^{\gamma\text{-}\alpha\beta}_{E\rightarrow TP}$):

a. After turning off the interactions between γ subunit and the C-terminal domains of $\alpha_3\beta_3$ hexamer, $C^{\gamma\text{-}\alpha\beta}_{E\rightarrow TP}$

Table III
Key Residues Involved in Two Correlations: $C^{\gamma\text{-}\beta}_{HO\rightarrow E}$—Between the Hinge-Bending Motion $\beta_{HO} \rightarrow \beta_E$ and Counterclockwise γ Rotation; $C^{\gamma\text{-}\alpha\beta}_{E\rightarrow TP}$—Between the Intersubunit Rotation $\alpha_E-\beta_E \rightarrow \alpha_{TP}-\beta_{TP}$ and Counterclockwise γ Rotation

Correlation	Key residues
$C^{\gamma\text{-}\beta}_{HO\rightarrow E}$	β_E: 279
	α_E: 356, 357, 361, 402, 403, 404, 405, 406, 407, 410, 411, 420, 424, 427, 431
	β_{TP}: 395, 398
	β_{HO}: 137, 138, 172, 173, 174, 175, 199, 315, 337, 341, 342, 343, 344, 345, 379, 380, 383, 386, 389, 390, 391, 392, 394, 395, 396, 397, 398, 400, 401, 402, 404, 405, 408, 411, 412, 413, 417, 418, 423, 424, 425, 426, 431, 458, 459, 460
	α_{HO}: 143, 376, 379, 390, 391, 394, 397, 401, 405, 406, 408, 409, 410, 411, 416
	γ: 15, 19, 22, 23, 25, 29, 30, 81, 82, 83, 85, 86, 87, 88, 113, 115, 117, 120, 135, 233, 260
$C^{\gamma\text{-}\alpha\beta}_{E\rightarrow TP}$	β_E: 17, 18, 19, 32, 64, 65, 99, 158, 160, 188, 190, 222, 223, 224, 225, 226, 227, 268, 271, 279, 280, 314, 316, 317, 356
	α_E: 97, 182, 216, 221, 243, 283, 284, 287, 289, 291, 292, 293, 296, 297, 298, 299, 301, 330, 336, 338, 340, 346, 347, 361, 362, 363, 364, 375, 377, 402, 403, 404, 405, 406, 407, 410, 411, 417, 420, 424, 427, 431, 432, 434, 435
	β_{TP}: 390, 393, 394, 395, 398, 405
	α_{TP}: 174
	β_{HO}: 391, 392, 394, 395, 397, 400, 402
	α_{HO}: 405, 408, 411
	γ: 18, 22, 23, 25, 30, 81, 83, 85, 135, 259, 260, 263, 267

Residue numbering is of yeast F_1.

decreases sharply from 0.46 to −0.16. To identify which α or β subunit is involved in $C^{\gamma\text{-}\alpha\beta}_{E\rightarrow TP}$, we then turn off the interactions involving a selected α or β subunit. It is found that the largest decrease in $C^{\gamma\text{-}\alpha\beta}_{E\rightarrow TP}$ (from 0.46 to 0.22) occurs when the γ-α_E interactions are turned off. The γ-α_E interactions involve residues K18, T22, I25, T29, R30 of γ subunit, and A404, F405, D411 of α_E subunit (all of them are highly conserved with conservation score ≥ 8[89]). On the contrary, $C^{\gamma\text{-}\alpha\beta}_{E\rightarrow TP}$ slightly increases when the γ-β_{TP} or γ-β_{HO} interactions are turned off, which indicates that the γ-β interactions are not essential to $C^{\gamma\text{-}\alpha\beta}_{E\rightarrow TP}$.

b. After turning off the interactions between γ subunit and the ATP-binding domains of $\alpha_3\beta_3$ hexamer, $C^{\gamma\text{-}\alpha\beta}_{E\rightarrow TP}$ slightly increases to 0.49, which suggests that these interactions are not essential to $C^{\gamma\text{-}\alpha\beta}_{E\rightarrow TP}$.

The above results are consistent with experimental studies on the role of γ-β interactions in F_1 dynamics. Although the γ-β interactions involving the highly conserved DELSEED motif (residues 394–400) of C-terminal domain were highlighted as functionally important,[30] none of these amino acids are absolutely essential for catalysis.[95] In fact, complete elimination of the negative charges in the DELSEED motif did not affect the rotational characteristics of F_1.[96]

Following "Couplings between hinge-bending motions and γ subunit rotation" subsection, we have recalculated $C^{\gamma\text{-}\alpha\beta}_{E\rightarrow TP}$ for the γ-truncated F_1 structure [see Fig. 1(d)]. Compared with the γ-intact F_1 structure, this correlation slightly increases to 0.49, which suggests that it persists in the γ-truncated F_1 structure. This result, together with the result of "Couplings between hinge-bending motions and γ subunit rotation" subsection, strongly supports the conclusion that a rigid axle (corresponding to the lower part of γ subunit) is not required for rotational hydrolysis in F_1.[7] It also agrees with the findings that up to 12 C-terminal residues of γ subunit could be deleted without suppressing catalysis[97,98] or impairing γ rotation.[98]

Following "Couplings between hinge-bending motions and γ subunit rotation" subsection, we have analyzed how residue-position-specific perturbations (see Methods section) affect the correlation $C^{\gamma\text{-}\alpha\beta}_{E\rightarrow TP}$. It is found that the key residues involved in $C^{\gamma\text{-}\alpha\beta}_{E\rightarrow TP}$ are primarily clustered at the interfaces between the C-terminal domains of $\alpha_3\beta_3$ hexamer and γ subunit [see Fig. 4(c,d)]. Some are at α_E-β_E interface (including catalytic residues G160, G188 of β_E subunit and R375 of α_E subunit), which suggests that this correlation can be modulated by ATP binding at E-site. Some of these key residues were studied by mutations. For example, *E. coli* mutants αP281L[84] (corresponding to P291 of yeast F_1), αS347F[99] (corresponding to S346 of yeast F_1), αR376C[84,99] (corresponding to R375 of yeast F_1), βM209I (corresponding to M222 of yeast F_1),[100] and a mutant of βR182[101] (corresponding to R190 of yeast F_1) were defective in catalytic cooperativity. An *E. coli* mutant βD302E (corresponding to D316 of yeast F_1) was defective in F_1 assembly.[102] An *E. coli* double mutant βP403S (corresponding to P417 of yeast F_1) and βG415D had impaired ATPase activity.[103] A bovine mutant βE395A (corresponding to E395 of yeast F_1) showed a five-fold decrease in ATPase activity.[96] Further mutational studies will validate the prediction that these key residues couple ATP binding with γ rotation.

The finding of significant coupling between counterclockwise γ rotation and α_E-$\beta_E \rightarrow \alpha_{TP}$-$\beta_{TP}$ instead of $\beta_E \rightarrow \beta_{TP}$ supports the importance of α_E-$\beta_E \rightarrow \alpha_{TP}$-$\beta_{TP}$ to ATP-binding-driven γ rotation. Although the closing hinge-bending motion can be induced by both ATP binding and ADP binding, only ATP binding is coupled to the α_E-$\beta_E \rightarrow \alpha_{TP}$-$\beta_{TP}$ rotation (no rigid-body rotation from α_E-β_E to α_{HO}-β_{HO}). In the "binding-zipper" model,[104] it was postulated that hydrogen bonds between ATP and P loop are progressively formed to drive the closing hinge-bending motion in β_E subunit that pushes γ subunit to rotate in counterclockwise direction. This scenario may need to be revised to incorporate the intersubunit rotation triggered by ATP binding. The α_E-$\beta_E \rightarrow \alpha_{TP}$-$\beta_{TP}$ rotation could reposition α_E and β_E subunits relative to γ subunit to facilitate a biased coupling between the closing of β subunit and counterclockwise γ rotation.

CONCLUSIONS

In summary, our modeling of allosteric couplings has revealed the following order of structural events during the cyclic structural transition of F_1: ATP binding closes the E-site (E → TP) and triggers two domain motions ($\beta_E \rightarrow \beta_{TP}$ and α_E-$\beta_E \rightarrow \alpha_{TP}$-$\beta_{TP}$); the latter is coupled to the counterclockwise rotation of γ subunit, which is subsequently coupled to the opening of β_{HO} subunit ($\beta_{HO} \rightarrow \beta_E$); the remaining local motions at catalytic sites (HO → E, TP → HO) and domain motion (α_{TP}-$\beta_{TP} \rightarrow \alpha_{HO}$-$\beta_{HO}$) associated with product release and hydrolysis occur at the late stage of the transition.

This study offers a new perspective to the conflicting results from two recent coarse-grained simulations of the structural transitions in F_1 during hydrolysis[24,53]:

a. We have found a strong coupling between the opening of β_{HO} subunit and counterclockwise γ rotation at the early stage of the cyclic structural transition, which increases when the interactions between γ subunit and the C-terminal domain of β_{HO} subunit are abolished (see "Couplings between hinge-bending motions and γ subunit rotation" subsection). This result is consistent with the finding that γ rotation is obstructed by a closed β_{HO} conformation.[53] However, our interpretation differs from Ref. 53. Considering that the opening of β_{HO} subunit is energy-requiring,[33] it is more likely to result from rather than cause the counterclockwise rotation of γ subunit.[53]
b. Our finding of early occurrence of the closing of β_E subunit (see "Couplings between hinge-bending motions and catalytic sites" subsection) and the opening of β_{HO} subunit (see "Couplings between hinge-bending motions and γ subunit rotation" subsection) during the cyclic structural transition also agrees with Ref. [53]. However, this result is not interpreted as simultaneous ATP binding and product release.[53] On the contrary, because the closing of E-site precedes the opening of HO-site (see "Couplings between hinge-bending motions and catalytic sites" subsection), a structural intermediate with tri-site nucleotide occupancy[43] may exist between ATP binding and product release.
c. Our NMA is (see "Low-frequency modes collectively capture the cyclic conformational change in F_1" section), correlation analysis (see "Correlation analysis of allosterically coupled motions in F_1" section) and preliminary transition pathway modeling (unpublished data) broadly agree with the proposal[24] that ATP binding causes a conformational transition to an intermediate structure[25] (PDB: 1H8E) with β_E subunit closed ($\beta_E \rightarrow \beta_{TP}$) and β_{HO} subunit half-closed ($\beta_{HO} \rightarrow \beta_{HC}$).

Based on the modeling results we have made the following predictions for experimental tests. First, we have identified key amino acid residues involved in the allosteric couplings in F_1. Perturbations to these residues are predicted to compromise cooperative ATPase in F_1. Indeed, some of them were already verified by past mutational studies. In particular, our results agree with the recent finding that a γ-truncated F_1 retains its rotational catalysis.[7] Second, we have predicted that ATP binding at E-site precedes product release at HO-site, which can be tested by trapping an intermediate state following ATP binding and prior to ADP release. Indeed, a bovine F_1 crystal structure was solved with all three catalytic sites occupied,[25] which may have captured such an F_1 intermediate.[24]

The rotational catalysis of F_1 has been a prototype for mechanistic models of many other hexameric motors including various hexameric helicases[2,3] and AAA+ motors.[4] Similar to F_1, these hexameric motors share structurally similar core NTP-binding domains and undergo large nucleotide-dependent conformational changes. Our modeling methods will be applied to those hexameric motors in the future to explore mechanistic details of the allosteric couplings underlying the cooperative NTPase in these motors.

REFERENCES

1. Abrahams JP, Leslie AG, Lutter R, Walker JE. Structure at 2.8 A resolution of F1-ATPase from bovine heart mitochondria. Nature 1994;370:621–628.
2. Patel SS, Picha KM. Structure and function of hexameric helicases. Annu Rev Biochem 2000;69:651–697.
3. Donmez I, Patel SS. Mechanisms of a ring shaped helicase. Nucleic Acids Res 2006;34:4216–4224.
4. Snider J, Houry WA. AAA+ proteins: diversity in function, similarity in structure. Biochem Soc Trans 2008;36 (Part 1):72–77.
5. Nakamoto RK, Baylis Scanlon JA, Al-Shawi MK. The rotary mechanism of the ATP synthase. Arch Biochem Biophys 2008; 476:43–50.
6. Gibbons C, Montgomery MG, Leslie AGW, Walker JE. The structure of the central stalk in bovine F1-ATPase at 2.4 Å resolution. Nat Struct Biol 2000;7:1055–1061.
7. Furuike S, Hossain MD, Maki Y, Adachi K, Suzuki T, Kohori A, Itoh H, Yoshida M, Kinosita K, Jr. Axle-less F1-ATPase rotates in the correct direction. Science 2008;319:955–958.
8. Walker JE, Saraste M, Runswick MJ, Gay NJ. Distantly related sequences in the alpha- and beta-subunits of ATP synthase, myosin, kinases and other ATP-requiring enzymes and a common nucleotide binding fold. EMBO J 1982;1:945–951.
9. Noji H, Yasuda R, Yoshida M, Kinosita K, Jr. Direct observation of the rotation of F1-ATPase. Nature 1997;386:299–302.
10. Diez M, Zimmermann B, Börsch M, König M, Schweinberger E, Steigmiller S, Reuter R, Felekyan S, Kudryavtsev V, Seidel CA, Gräber P. Proton-powered subunit rotation in single membrane-bound F0F1-ATP synthase. Nat Struct Mol Biol 2004;11:135–141.
11. Cross RL, Grubmeyer C, Penefsky HS. Mechanism of ATP hydrolysis by beef heart mitochondrial ATPase. Rate enhancements resulting from cooperative interactions between multiple catalytic sites. J Biol Chem 1982;257:12101–12105.
12. Gresser MJ, Myers JA, Boyer PD. Catalytic site cooperativity of beef heart mitochondrial F1 adenosine triphosphatase. Correla-

tions of initial velocity, bound intermediate, and oxygen exchange measurements with an alternating three-site model. J Biol Chem 1982;257:12030–12038.
13. Grubmeyer C, Cross RL, Penefsky HS. Mechanism of ATP hydrolysis by beef heart mitochondrial ATPase. Rate constants for elementary steps in catalysis at a single site. J Biol Chem 1982;257:12092–12100.
14. Kayalar C, Rosing J, Boyer PD. An alternating site sequence for oxidative phosphorylation suggested by measurement of substrate binding patterns and exchange reaction inhibitions. J Biol Chem 1977;252:2486–2491.
15. Falson P, Goffeau A, Boutry M, Jault JM. Structural insight into the cooperativity between catalytic and noncatalytic sites of F1-ATPase. Biochim Biophys Acta 2004;1658:133–140.
16. Boyer PD. The binding change mechanism for ATP synthase–some probabilities and possibilities. Biochim Biophys Acta 1993;1140:215–250.
17. Milgrom YM, Murataliev MB, Boyer PD. Bi-site activation occurs with the native and nucleotide-depleted mitochondrial F1-ATPase. Biochem J 1998;330:1037–1043.
18. Milgrom YM, Cross RL. Rapid hydrolysis of ATP by mitochondrial F1-ATPase correlates with the filling of the second of three catalytic sites. Proc Natl Acad Sci USA 2005;102:13831–13836.
19. Weber J, Wilke-Mounts S, Lee RS, Grell E, Senior AE. Specific placement of tryptophan in the catalytic sites of *Escherichia coli* F1-ATPase provides a direct probe of nucleotide binding: maximal ATP hydrolysis occurs with three sites occupied. J Biol Chem 1993;268:20126–20133.
20. Weber J, Senior AE. ATP synthase: what we know about ATP hydrolysis and what we do not know about ATP synthesis. Biochim Biophys Acta 2000;1458:300–309.
21. Penefsky HS. Rate constants and equilibrium constants for the elementary steps of ATP hydrolysis by beef heart mitochondrial ATPase. Methods Enzymol 1986;126:608–619.
22. Senior AE. J Bioenerg Biomembr 1992;24:479–484.
23. Bowler MW, Montgomery MG, Leslie AG, Walker JE. How azide inhibits ATP hydrolysis by the F-ATPases. Proc Natl Acad Sci USA 2006;103:8646–8649.
24. Pu J, Karplus M. How subunit coupling produces the gamma-subunit rotary motion in F1-ATPase. Proc Natl Acad Sci USA 2008;105:1192–1197.
25. Menz RI, Walker JE, Leslie AG. Structure of bovine mitochondrial F(1)-ATPase with nucleotide bound to all three catalytic sites: implications for the mechanism of rotary catalysis. Cell 2001;106:331–341.
26. Kabaleeswaran V, Puri N, Walker JE, Leslie AG, Mueller DM. Novel features of the rotary catalytic mechanism revealed in the structure of yeast F1 ATPase. EMBO J 2006;25:5433–5442.
27. Cross RL. The mechanism and regulation of ATP synthesis by F1-ATPases. Annu Rev Biochem 1981;50:681–714.
28. Senior AE, Nadanaciva S, Weber J. The molecular mechanism of ATP synthesis by F1F0-ATP synthase. Biochim Biophys Acta 2002;1553:188–211.
29. Weber J, Senior AE. ATP synthesis driven by proton transport in F1F0-ATP synthase. FEBS Lett 2003;545:61–70.
30. Nakamoto RK, Ketchum CJ, Al-Shawi MK. Rotational coupling in the F0F1 ATP synthase. Annu Rev Biophys Biomol Struct 1999;28:205–234.
31. Mao HZ, Weber J. Identification of the betaTP site in the X-ray structure of F1-ATPase as the high-affinity catalytic site. Proc Natl Acad Sci USA 2007;104:18478–18483.
32. Scanlon JA, Al-Shawi MK, Le NP, Nakamoto RK. Determination of the partial reactions of rotational catalysis in F1-ATPase. Biochemistry 2007;46:8785–8797.
33. Yang W, Gao YQ, Cui Q, Ma J, Karplus M. The missing link between thermodynamics and structure in F1-ATPase. Proc Natl Acad Sci USA 2003;100:874–879.
34. Yasuda R, Noji H, Kinosita K, Jr, Yoshida M. F1-ATPase is a highly efficient molecular motor that rotates with discrete 120 steps. Cell 1998;93:1117–1124.
35. Adachi K, Yasuda R, Noji H, Itoh H, Harada Y, Yoshida M, Kinosita K, Jr. Stepping rotation of F1-ATPase visualized through angle-resolved single-fluorophore imaging. Proc Natl Acad Sci USA 2000;97:7243–7247.
36. Yasuda R, Noji H, Yoshida M, Kinosita K, Itoh H. Resolution of distinct rotational substeps by submillisecond kinetic analysis of F1-ATPase. Nature 2001;410:898–904.
37. Nishizaka T, Oiwa K, Noji H, Kimura S, Muneyuki E, Yoshida M, Kinosita K, Jr. Chemomechanical coupling in F1-ATPase revealed by simultaneous observation of nucleotide kinetics and rotation. Nat Struct Mol Biol 2004;11:142–148.
38. Shimabukuro K, Muneyuki E, Yoshida M. An alternative reaction pathway of F1-ATPase suggested by rotation without 80 degrees/40 degrees substeps of a sluggish mutant at low ATP. Biophys J 2006;90:1028–1032.
39. Shimabukuro K, Yasuda R, Muneyuki E, Hara KY, Kinosita K, Jr, Yoshida M. Catalysis and rotation of F1 motor: cleavage of ATP at the catalytic site occurs in 1 ms before 40 degree substep rotation. Proc Natl Acad Sci USA 2003;100:14731–14736.
40. Ariga T, Muneyuki E, Yoshida M. F1-ATPase rotates by an asymmetric, sequential mechanism using all three catalytic subunits. Nat Struct Mol Biol 2007;14:841–846.
41. Adachi K, Oiwa K, Nishizaka T, Furuike S, Noji H, Itoh H, Yoshida M, Kinosita K, Jr. Coupling of rotation and catalysis in F(1)-ATPase revealed by single-molecule imaging and manipulation. Cell 2007;130:309–321.
42. Watanabe R, Iino R, Shimabukuro K, Yoshida M, Noji H. Temperature-sensitive reaction intermediate of F1-ATPase. EMBO Rep 2008;9:84–90.
43. Weber J, Senior AE. Catalytic mechanism of F1-ATPase. Biochim Biophys Acta 1997;1319:19–58.
44. Wang H, Oster G. Energy transduction in F1 motor of ATP synthase. Nature 1998;396:279–282.
45. Sun SX, Wang H, Oster G. Asymmetry in the F1-ATPase and its implications for the rotational cycle. Biophys J 2004;86:1373–1384.
46. Gao Y, Yang W, Marcus RA, Karplus M. A model for the cooperative free energy transduction and kinetics of ATP hydrolysis by F1-ATPase. Proc Natl Acad Sci USA 2003;100:11339–11344.
47. Dittrich M, Hayashi S, Schulten K. On the mechanism of ATP hydrolysis in F1-ATPase. Biophys J 2003;85:2253–2266.
48. Dittrich M, Hayashi S, Schulten K. ATP hydrolysis in the betaTP and betaDP catalytic sites of F1-ATPase. Biophys J 2004;87:2954–2967.
49. Böckmann RA, Grubmüller H. Nanoseconds molecular dynamics simulation of primary mechanical energy transfer steps in F1-ATP synthase. Nat Struct Biol 2002;9:198–202.
50. Böckmann RA, Grubmüller H. Conformational dynamics of the F1-ATPase beta-subunit: a molecular dynamics study. Biophys J 2003;85:1482–1491.
51. Ma J, Flynn TC, Cui Q, Leslie AG, Walker JE, Karplus M. A dynamic analysis of the rotation mechanism for conformational change in F(1)-ATPase. Structure 2002;10:921–931.
52. Antes I, Chandler D, Wang H, Oster G. The unbinding of ATP from F1-ATPase. Biophys J 2003;85:695–706.
53. Koga N, Takada S. Folding-based molecular simulations reveal mechanisms of the rotary motor F1-ATPase. Proc Natl Acad Sci USA 2006;103:5367–5372.
54. Tozzini V. Coarse-grained models for proteins. Curr Opin Struct Biol 2005;15:144–150.
55. Go N. Theoretical studies of protein folding. Annu Rev Biophys Bioeng 1983;12:183–210.
56. Onuchic JN, Wolynes PG. Theory of protein folding. Curr Opin Struct Biol 2004;14:70–75.

57. Tirion MM. Large amplitude elastic motions in proteins from a single-parameter. Atom Anal Phys Rev Lett 1996;77:1905–1908.
58. Haliloglu T, Bahar I, Erman B. Gaussian dynamics of folded proteins. Phys Rev Lett 1997;79:3090–3093.
59. Bahar I, Atilgan AR, Erman B. Direct evaluation of thermal fluctuations in proteins using a single-parameter harmonic potential. Fold Des 1997;2:173–181.
60. Hinsen K. Analysis of domain motions by approximate normal mode calculations. Proteins 1998;33:417–429.
61. Atilgan AR, Durell SR, Jernigan RL, Demirel MC, Keskin O, Bahar I. Anisotropy of fluctuation dynamics of proteins with an elastic network model. Biophys J 2001;80:505–515.
62. Tama F, Sanejouand YH. Conformational change of proteins arising from normal mode calculations. Protein Eng 2001;14:1–6.
63. Krebs WG, Alexandrov V, Wilson CA, Echols N, Yu H, Gerstein M. Normal mode analysis of macromolecular motions in a database framework: developing mode concentration as a useful classifying statistic. Proteins 2002;48:682–695.
64. Bahar I, Rader AG. Coarse-grained normal mode analysis in structural biology. Curr Opin Struct Biol 2005;15:586–592.
65. Ma JP. Usefulness and limitations of normal mode analysis in modeling dynamics of biomolecular complexes. Structure 2005;13:373–380.
66. Tama F, Brooks CL. Symmetry, form, and shape: guiding principles for robustness in macromolecular machines. Annu Rev Biophys Biomol Struct 2006;35:115–133.
67. Tama F, Valle M, Frank J, Brooks CL. Dynamic reorganization of the functionally active ribosome explored by normal mode analysis and cryo-electron microscopy. Proc Natl Acad Sci USA 2003;100:9319–9323.
68. Wang Y, Rader AJ, Bahar I, Jernigan RL. Global ribosome motions revealed with elastic network model. J Struct Biol 2004;147:302–314.
69. Keskin O, Bahar I, Flatow D, Covell DG, Jernigan RL. Molecular mechanisms of chaperonin GroEL-GroES function. Biochemistry 2002;41:491–501.
70. Zheng W, Brooks BR, Thirumalai D. Allosteric transitions in the chaperonin GroEL are captured by a dominant normal mode that is most robust to sequence variations. Biophys J 2007;93:2289–2299.
71. Tama F, Brooks CL. Diversity and identity of mechanical properties of icosahedral viral capsids studied with elastic network normal mode analysis. J Mol Biol 2005;345:299–314.
72. Rader AJ, Vlad DH, Bahar I. Maturation dynamics of HK97 bacteriophage capsid. Structure 2005;13:413–421.
73. Boyer PD. Catalytic site occupancy during ATP synthase catalysis. FEBS Lett 2002;512:29–32.
74. Zheng W, Brooks BR. Identification of dynamical correlations within the myosin motor domain by the normal mode analysis of an elastic network model. J Mol Biol 2005;346:745–759.
75. Zheng W, Brooks BR, Doniach S, Thirumalai D. Network of dynamically important residues in the open/closed transition in polymerases is strongly conserved. Structure 2005;13:565–577.
76. Shirakihara Y, Leslie AG, Abrahams JP, Walker JE, Ueda T, Sekimoto Y, Kambara M, Saika K, Kagawa Y, Yoshida M. The crystal structure of the nucleotide-free alpha 3 beta 3 subcomplex of F1-ATPase from the thermophilic Bacillus PS3 is a symmetric trimer. Structure 1997;5:825–836.
77. Bianchet MA, Hullihen J, Pedersen PL, Amzel LM. The 2.8-A structure of rat liver F1-ATPase: configuration of a critical intermediate in ATP synthesis/hydrolysis. Proc Natl Acad Sci USA 1998;95:11065–11070.
78. Yasuda R, Masaike T, Adachi K, Noji H, Itoh H, Kinosita K, Jr. The ATP-waiting conformation of rotating F1-ATPase revealed by single-pair fluorescence resonance energy transfer. Proc Natl Acad Sci USA 2003;100:9314–9318.
79. Kagawa R, Montgomery MG, Braig K, Leslie AG, Walker JE. The structure of bovine F1-ATPase inhibited by ADP and beryllium fluoride. EMBO J 2004;23:2734–2744.
80. Kinosita K, Adachi K, Itoh H. Rotation of F1-ATPase: how an ATP-driven molecular machine may work. Annu Rev Biophys Biomol Struct 2004;33:245–268.
81. Liu MS, Todd BD, Sadus RJ. Dynamic and coordinating domain motions in the active subunits of the F1-ATPase molecular motor. Biochim Biophys Acta 2006;1764:1553–1560.
82. Futai M, Noumi T, Maeda M. ATP synthase (H+-ATPase): results by combined biochemical and molecular biological approaches. Annu Rev Biochem 1989;58:111–136.
83. Nadanaciva S, Weber J, Wilke-Mounts S, Senior AE. Importance of F1-ATPase residue alpha-Arg-376 for catalytic transition state stabilization. Biochemistry 1999;38:15493–15499.
84. Soga S, Noumi T, Takeyama M, Maeda M, Futai M. Mutational replacements of conserved amino acid residues in the alpha subunit change the catalytic properties of *Escherichia coli* F1-ATPase. Arch Biochem Biophys 1989;268:643–648.
85. Turina P, Aggeler R, Lee RS, Senior AE, Capaldi RA. The cysteine introduced into the a subunit of the *Escherichia coli* F1-ATPase by the mutation αR376C is near the α-β subunit interface and close to a noncatalytic nucleotide binding site. J Biol Chem 1993;268:6978–6984.
86. Cui Q, Li G, Ma J, Karplus M. A normal mode analysis of structural plasticity in the biomolecular motor F(1)-ATPase. J Mol Biol 2004;340:345–372.
87. Al-Shawi MK, Nakamoto RK. Mechanism of energy coupling in the FOF1-ATP synthase: the uncoupling mutation, gammaM23K, disrupts the use of binding energy to drive catalysis. Biochemistry 1997;36:12954–12960.
88. Ren H, Allison WS. On what makes the gamma subunit spin during ATP hydrolysis by F(1). Biochim Biophys Acta 2000;1458:221–233.
89. Glaser F, Rosenberg Y, Kessel A, Pupko T, Ben-Tal N. The ConSurf-HSSP database: the mapping of evolutionary conservation among homologs onto PDB structures. Proteins 2005;58:610–617.
90. Iwamoto A, Park MY, Maeda M, Futai M. Domains near ATP (c phosphate in the catalytic site of H+-ATPase. Model proposed from mutagenesis and inhibitor studies. J Biol Chem 1993;268:3156–3160.
91. Omote H, Park MY, Maeda M, Futai M. The alpha/beta subunit interaction in H(+)-ATPase (ATP synthase). An *Escherichia coli* alpha subunit mutation (Arg-alpha 296–>Cys) restores coupling efficiency to the deleterious beta subunit mutant (Ser-beta 174–>Phe). J Biol Chem 1994;269:10265–10269.
92. Iko Y, Sambongi Y, Tanabe M, Iwamoto-Kihara A, Saito K, Ueda I, Wada Y, Futai M. ATP synthase F(1) sector rotation. Defective torque generation in the beta subunit Ser-174 to Phe mutant and its suppression by second mutations. J Biol Chem 2001;276:47508–47511.
93. Masaike T, Mitome N, Noji H, Muneyuki E, Yasuda R, Kinosita K, Yoshida M. Rotation of F(1)-ATPase and the hinge residues of the beta subunit. J Exp Biol 2000;203:1–8.
94. Boltz KW, Frasch WD. Hydrogen bonds between the alpha and beta subunits of the F1-ATPase allow communication between the catalytic site and the interface of the beta catch loop and the gamma subunit. Biochemistry 2006;45:11190–11199.
95. Ketchum CJ, Al-Shawi MK, Nakamoto RK. Intergenic suppression of the gammaM23K uncoupling mutation in F0F1 ATP synthase by betaGlu-381 substitutions: the role of the beta380DELSEED386 segment in energy coupling. Biochem J 1998;330:707–712.
96. Hara KY, Noji H, Bald D, Yasuda R, Kinosita K, Yoshida M. The role of the DELSEED motif of the beta subunit in rotation of F1-ATPase. J Biol Chem 2000;275:14260–14263.

97. Iwamoto A, Miki J, Maeda M, Futai M. H(+)-ATPase gamma subunit of *Escherichia coli*. Role of the conserved carboxyl-terminal region. J Biol Chem 1990;265:5043–5048.
98. Müller M, Pänke O, Junge W, Engelbrecht S. F1-ATPase, the C-terminal end of subunit gamma is not required for ATP hydrolysis-driven rotation. J Biol Chem 2002;277:23308–23313.
99. Maggio MB, Pagan J, Parsonage D, Hatch L, Senior AE. The defective proton-ATPase of uncA mutants of *Escherichia coli*. Identification by DNA sequencing of residues in the alpha-subunit which are essential for catalysis or normal assembly. J Biol Chem 1987;262:8981–8984.
100. Parsonage D, Duncan TM, Wilke-Mounts S, Kironde FA, Hatch L, Senior AE. The defective proton-ATPase of uncD mutants of *Escherichia coli*. Identification by DNA sequencing of residues in the beta-subunit which are essential for catalysis or normal assembly. J Biol Chem 1987;262:6301–6307.
101. Senior AE, Weber J, Nadanaciva S. The catalytic transition state in ATP synthase. J Bioenerg Biomembr 2000;32:523–529.
102. Omote H, Tainaka K, Fujie K, Iwamoto-Kihara A, Wada Y, Futai M. Stability of the *Escherichia coli* ATP synthase F0F1 complex is dependent on interactions between gamma Gln-269 and the beta subunit loop beta Asp-301-beta Asp-305. Arch Biochem Biophys 1998;358:277–282.
103. Kironde FA, Parsonage D, Senior AE. Random mutagenesis of the gene for the beta-subunit of F1-ATPase from *Escherichia coli*. Biochem J 1989;259:421–426.
104. Oster G, Wang H. Why is the mechanical efficiency of F1-ATPase so high? J Bioenerg Biomembr 2000;32:459–469.